

# New solution to the hyperon puzzle of neutron stars: Quantum many-body effects

Hao-Fu Zhu,<sup>1,2</sup> Guo-Zhu Liu,<sup>3,\*</sup> Xufen Wu,<sup>1,2</sup> and Ye-Fei Yuan<sup>1,2</sup>

<sup>1</sup>*Department of Astronomy, University of Science and Technology of China, Hefei, Anhui 230026, China*

<sup>2</sup>*School of Astronomy and Space Science, University of Science and Technology of China, Hefei, Anhui 230026, China*

<sup>3</sup>*Department of Modern Physics and Anhui Center for fundamental sciences in theoretical physics, University of Science and Technology of China, Hefei, Anhui 230026, China*

The hyperon puzzle refers to the challenge of reconciling the existence of hyperons in neutron star cores and the observed high masses of neutron stars. The recent discovery of PSR J0952-0607 ( $2.35 \pm 0.17 M_{\odot}$ ) has intensified this challenge. Existing solutions fail to achieve such a high mass, and often predict unrealistically fast cooling that is at odds with observations. Here, we propose a novel solution to the hyperon puzzle. Using the Dyson-Schwinger equation approach, we incorporate the quantum many-body effects caused by strong baryon-meson interactions into the equation of state for cold baryonic matter and find it stiff enough to support a maximum hyperon-star mass of  $M_{\max} \approx 2.59 M_{\odot}$ , which can explain all the observed high neutron-star masses. The resulting proton and hyperon fractions are remarkably low, thus the nucleonic and hyperonic direct Urca processes are significantly suppressed. As a result, fast cooling typically does not occur in ordinary neutron stars.

## I. INTRODUCTION

Neutron stars (NSs) provide a unique platform for exploring the intriguing behaviors of dense matter [1, 2]. The baryon density in their inner cores can be several times higher than the nuclear saturation density  $n_{\text{Bo}}$ , offering extreme conditions unattainable in all terrestrial laboratories. In particular, hyperons - baryons with strange quark content - have long been conjectured to exist in NS cores due to  $\beta$ -equilibrium [3–8]. It is widely recognized that NSs present the most promising environment for studying the physical effects of hyperons.

The Walecka-type relativistic mean-field theory (RMFT) [4, 9–11] has demonstrated remarkable success in describing both finite nuclei [12–16] and nuclear matter [13, 15–18]. Consequently, it has become the most frequently employed method of calculating the equation of state (EOS) of NS matter, reliably reproducing a wide range of astronomical observations [18–22]. Extensive early studies based on this method have revealed that the EOSs are significantly softened after including hyperons [4–8, 23]. This reduces the maximum NS mass  $M_{\max}$  down to values lower than  $2.0 M_{\odot}$ , where  $M_{\odot}$  is the solar mass. Since 2010, several NSs with masses exceeding  $2.0 M_{\odot}$  have been observed. Notable examples include PSR J1614-2230 with a mass of  $1.97 \pm 0.04 M_{\odot}$  [24], PSR J0348+0432 with a mass of  $2.01 \pm 0.04 M_{\odot}$  [25], and PSR J0740+6620 with a mass of  $2.08 \pm 0.07 M_{\odot}$  [26]. It is difficult to reconcile the observations of these massive NSs with the hypothesized existence of hyperons. This mass problem is termed the hyperon puzzle in the NS community [27–54].

Many possible solutions [38–54] have been proposed to address the hyperon puzzle. Generically, these solutions fall into two main categories. The first category assumes

the appearance of novel degrees of freedom, such as hybrid hadron-quark phases [38–40] or  $\Delta$  isobar [41–44], which can delay the emergence of hyperons until higher densities are reached. The second one focuses on refining the description of hyperon-involved interactions or exploring extra repulsive interactions to stiffen the hyperon star (HS) EOS [45–54]. With such manipulations, the maximum mass can be lifted to values slightly larger than  $2.0 M_{\odot}$ . However, despite these advancements, the hyperon puzzle remains unsettled, as the maximum mass computed within RMFT still falls short of the observed NS values. This puzzle has been further complicated by the recent discovery of the supermassive “black-widow” pulsar PSR J0952-0607, whose mass  $2.35 \pm 0.17 M_{\odot}$  [55] is subject to large uncertainty because its determination relies on a number of more complex, model-dependent astrophysical assumptions than those for NSs in white dwarf binaries.

In addition to the mass discrepancy mentioned above, the hyperon puzzle usually entails a cooling inconsistency [30]. While some specific RMFT models can support NS masses in the range of  $2.2 M_{\odot} - 2.3 M_{\odot}$ , their consistency with thermal-evolution observations of NSs remains an open issue [30]. Within RMFT, the symmetry energy of NS matter tends to increase rapidly with growing baryon density. This behavior results in a low threshold density  $n_{\text{nDU}}$  and, consequently, a low threshold NS mass  $M_{\text{nDU}}$  above which nucleonic direct Urca (DU) process [56], such as  $n \rightarrow p + e^- + \bar{\nu}_e$ , are activated in a baryon-matter core [19, 57–60]. Moreover, RMFT studies predict hyperon fractions much higher than the threshold value needed to trigger hyperonic DU processes [61], such as  $\Lambda \rightarrow p + e + \bar{\nu}_e$ . Even when the suppression from baryon pairing is taken into account [62, 63], the calculated NS cooling still proceeds markedly faster than observed, so HSs would become undetectable within few years, which contradicts astrophysical observations [30].

The limitations of current theoretical approaches may originate from the oversimplified nature of RMFT, which

\*Corresponding author: gzliu@ustc.edu.cn

cannot incorporate the impact of meson dynamics and quantum many-body effects induced by the baryon-meson interactions. A critical investigation is needed to examine whether including these essential features can provide satisfactory solutions to the above two aspects of the hyperon puzzle.

In this paper, we demonstrate that both the mass and cooling problems associated with hyperon puzzle may be resolved in a unified manner when quantum many-body effects are incorporated into the theoretical framework. Based on the Dyson-Schwinger (DS) equation approach illustrated in a previous publication [64], we carry out a quantum field-theoretical study of the strong baryon-meson interactions. The inclusion of many-body effects leads to sufficiently stiff EOSs that permit the existence of hyperons in the NS interior and support a maximum mass  $M_{\max} \approx 2.59M_{\odot}$ , which is high enough to account for all the observed NS masses. We calculate the resulting proton and hyperon fractions and show that they are all remarkably low, even in the high density regions. This prohibits nucleonic DU process and also substantially suppresses hyperonic DU processes. Consequently, in our scenario, the HSs normally do not experience rapid cooling, provided that superfluid and superconductivity are not considered [65–67]. Our results provide a new perspective on the internal structure of NSs and reveal the crucial role of quantum many-body effects.

The rest of the paper is organized as follows. In II, we present the effective model of the HS matter and derive the self-consistent integral equations for three renormalization functions that account for quantum many-body effects. In III, we evaluate the NS EOS and HS EOS based on the numerical solutions of renormalization functions. In IV, we determine the maximum HS mass for several different values of the symmetry energy slope. In V, we show the results of particle fractions and analyze their physical influence on the fate of HS cooling rate. A brief summary is given in VI.

## II. MODEL OF NS MATTER

As an extension of a previous work [64], we describe the physics of NS matter through an effective quantum hadrodynamics model in which the baryons are coupled to three sorts of mesons [64], including neutral  $\sigma$  mesons, denoted by an isoscalar scalar field  $\sigma$ , neutral vector  $\omega$  mesons, denoted by an isoscalar vector field  $\omega_{\mu} = (\omega_0, \omega_1, \omega_2, \omega_3)$ , and charged vector  $\rho$  mesons, denoted by an isovector vector field  $\rho_{\mu} = (\rho_{\mu}^1, \rho_{\mu}^2, \rho_{\mu}^3)$  with  $\rho_{\mu}^i = (\rho_0^i, \rho_1^i, \rho_2^i, \rho_3^i)$ . Considering the rotational invariance around the third axis in isospin space, we only retain the isospin three-component of  $\rho_{\mu}^3$ , namely the neutral  $\rho^0$  mesons. Such a  $\sigma$ - $\omega$ - $\rho$  model is represented by the following Lagrangian density

$$\mathcal{L} = \mathcal{L}_{\text{Baryon}} + \mathcal{L}_{\text{meson}} + \mathcal{L}_{\text{lepton}}, \quad (1)$$

where

$$\begin{aligned} \mathcal{L}_{\text{Baryon}} &= \sum_{\text{B}} \bar{\psi}_{\text{B}} (i\partial_{\mu} \gamma^{\mu} - m_{\text{B}} + g_{\sigma \text{B}} \sigma - g_{\omega \text{B}} \omega_{\mu} \gamma^{\mu} \\ &\quad - \Gamma_{\rho \text{B}} \rho_{\mu}^3 I_{3\text{B}} \gamma^{\mu}) \psi_{\text{B}}, \\ \mathcal{L}_{\text{meson}} &= \frac{1}{2} \partial_{\mu} \sigma \partial^{\mu} \sigma - \frac{1}{2} m_{\sigma}^{*2} \sigma^2 - \frac{1}{4} \omega_{\mu\nu} \omega^{\mu\nu} \\ &\quad + \frac{1}{2} m_{\omega}^2 \omega_{\mu} \omega^{\mu} - \frac{1}{4} \rho_{\mu\nu}^3 \rho^{3\mu\nu} + \frac{1}{2} m_{\rho}^2 \rho_{\mu}^3 \rho^{3\mu}, \\ \mathcal{L}_{\text{lepton}} &= \sum_l \bar{\psi}_l (i\partial_{\mu} \gamma^{\mu} - m_l) \psi_l, \end{aligned} \quad (2)$$

where  $\partial_{\mu} = (\partial_t, \boldsymbol{\partial})$ ,  $\gamma^{\mu} = (\gamma^0, \boldsymbol{\gamma})$ ,  $\omega_{\mu\nu} = \partial_{\mu} \omega_{\nu} - \partial_{\nu} \omega_{\mu}$ , and  $\rho_{\mu\nu}^3 = \partial_{\mu} \rho_{\nu}^3 - \partial_{\nu} \rho_{\mu}^3$ . The spinor  $\psi_{\text{B}}$ , whose conjugate is  $\bar{\psi}_{\text{B}} = \psi_{\text{B}}^{\dagger} \gamma^0$ , has four components for baryonic matter, and the summation on B is over all the charge states of the baryon octet  $\text{B} = (n, p, \Lambda, \Sigma^+, \Sigma^-, \Sigma^0, \Xi^-, \Xi^0)$ . The baryons couple to  $\sigma$ ,  $\omega$ , and  $\rho^0$  mesons. The isospin projection in isospin-space is denoted by  $I_{3\text{B}} = \text{diag}(-\frac{1}{2}, \frac{1}{2}, 0, 1, -1, 0, -\frac{1}{2}, \frac{1}{2})$ , which is the matrix containing the isospin charges. Bare baryon masses are  $m_{n,p} = 939$  MeV,  $m_{\Lambda} = 1116$  MeV,  $m_{\Sigma^0,\pm} = 1193$  MeV, and  $m_{\Xi^{0,-}} = 1318$  MeV. Rest meson masses are  $m_{\sigma} = 550$  MeV,  $m_{\omega} = 783$  MeV, and  $m_{\rho} = 763$  MeV.  $m_{\sigma}^*$  denotes the renormalized mass of  $\sigma$ . Leptons  $\psi_l$ , where  $l = e^-, \mu^-$ , are included to ensure the  $\beta$ -equilibrium and electrical neutrality. The rest lepton masses are  $m_e = 0.511$  MeV and  $m_{\mu} = 105.7$  MeV.

The pronounced isospin asymmetry of NSs renders their properties, such as the crust structure, radius, tidal deformability, and the thresholds for DU processes, highly sensitive to the symmetry energy slope  $L_s$  [60, 64, 68–72], which is strongly influenced by isovector mesons. To systematically investigate how  $L_s$  affects properties of NSs, we introduce the density-dependent isovector coupling parameter  $\Gamma_{\rho \text{B}}$ , which has been widely adopted in density-dependent RMFT models [13, 16, 17, 72] and takes the form

$$\Gamma_{\rho \text{B}} = g_{\rho \text{B}} \exp \left[ -a_{\rho} \left( \frac{n_{\text{F}}^*}{n_{\text{B}0}} - 1 \right) \right]. \quad (3)$$

Here,  $g_{\rho \text{B}}$  is a density-independent coupling constant,  $n_{\text{F}}^*$  is the total baryon density, and  $a_{\rho}$  is a tuning parameter. At the nuclear saturation density  $n_{\text{F}}^* = n_{\text{B}0}$ ,  $\Gamma_{\rho \text{B}}$  reverts back to  $g_{\rho \text{B}}$ . Notably, the effective coupling of the  $\rho^0$  meson to baryons is governed by the product  $g_{\rho \text{B}} I_{3\text{B}}$ . Previous studies [64, 71, 72] have revealed that increasing  $a_{\rho}$  markedly lowers the symmetry energy slope  $L_s$ . A smaller  $L_s$  would soften the EOS of NS core, which yields more compact NSs in the intermediate-mass regime and leaves the maximum mass nearly unchanged. The other two nucleon-meson coupling constants  $g_{\sigma \text{B}}$  and  $g_{\omega \text{B}}$  are density independent.

In addition to baryon-meson couplings, mesons can couple to themselves and to each other through terms such as  $-g_3 \sigma^3$ ,  $-g_4 \sigma^4$ , and  $-g_{22} \sigma^2 \omega^2$ , etc. These nonlinear self- and cross-couplings appear in almost all RMFT

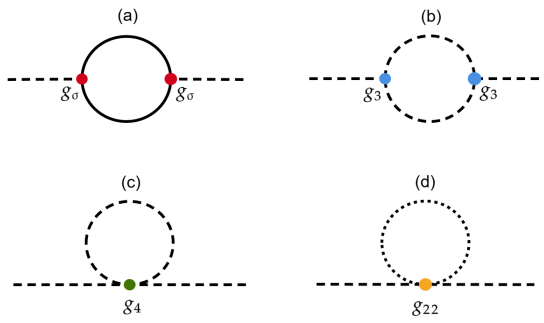


FIG. 1: Feynman diagrams for one-loop self-energy corrections to the  $\sigma$  meson mass. Solid line represents free baryon propagator. Dashed (dotted) line represents free  $\sigma$  ( $\omega$ ) meson propagator. Corrections of (a), (b), (c), and (d) come from baryon- $\sigma$  coupling, self-coupling  $g_3\sigma^3$ , self-coupling  $g_4\sigma^4$ , and cross-coupling  $g_{22}\sigma^2\omega^2$ , respectively.

models and play a crucial role in the determination of a realistic EOS. However, their coefficients are frequently negative, which can drive the thermodynamic potential unbounded from below and trigger an instability [4, 64]. We wish to retain the contributions of such nonlinear couplings while eliminating any risk of instability. According to the generic principles of quantum field theory, the main effects of meson self- and cross-couplings is the renormalization of bare meson masses. To illustrate this, consider the  $\sigma$  meson as an example. At one-loop level, its self-energy receives contributions from the baryon- $\sigma$  couplings and the nonlinear meson couplings, with the corresponding diagrams shown in Fig. 1. These corrections shift the bare  $\sigma$  mass  $m_\sigma$  to an effective renormalized mass  $m_\sigma^*$ , whose value depends on  $g_\sigma$ ,  $g_3$ ,  $g_4$ , and  $g_{22}$ . This implies that the influence of  $\sigma$  self-couplings and cross-couplings between  $\sigma$  and  $\omega$  meson is packaged into a single quantity  $m_\sigma^*$ . Guided by this consideration, we replace the bare mass  $m_\sigma$  in  $\mathcal{L}_{\text{meson}}$  by the renormalized mass  $m_\sigma^*$  from the outset and treat the ratio  $m_\sigma^*/m_\sigma$  as an adjusting parameter, whose value will be determined by fitting to nuclear saturation properties [64]. This substitution eliminates potential instability while packaging the physical effects of nonlinear meson interactions compactly into  $m_\sigma^*$ . At the same time,  $m_\sigma^*$  automatically incorporates the feedback of baryon- $\sigma$  coupling through the processes given by Fig. 1(a). The  $\omega$  and  $\rho^0$  masses can be modified by similar nonlinear couplings, but the modifications are numerically negligible since their bare masses ( $m_\omega$  and  $m_\rho$ ) are already quite large. We therefore fix  $m_\omega$  and  $m_\rho$  at their bare values.

Throughout the following calculations, NSs are treated as approximately at zero temperature, as the typical baryon Fermi energies ( $E_{\text{FB}} \approx 100 - 1000 \text{ MeV}$ ) in NSs far exceed the characteristic thermal energies ( $k_B T \approx 0.01 - 0.1 \text{ MeV}$ ). We anticipate that strong baryon-meson interactions will lead to significant quantum many-body effects, such as the Landau damping of baryons, the baryon velocity renormalization, and the baryon mass renormalization. To incorporate these effects into the

EOS, we will handle the model of Eq. (2) by employing the field-theoretical approach developed in [64]. The essence of this approach is to calculate the EOS based on the solutions of the DS equation of renormalized baryon propagator  $G_B(k)$ . As shown in [64],  $G_B(k)$  satisfies the following DS equation

$$\begin{aligned} G_B^{-1}(k) = & G_{B0}^{-1}(k) - ig_{\sigma B}^2 \int \frac{d^4 q}{(2\pi)^4} G_B(k+q) D_0(q) \\ & - ig_{\omega B}^2 \gamma_\mu \int \frac{d^4 q}{(2\pi)^4} G_B(k+q) F_0^{\mu\nu}(q) \gamma_\nu \\ & - i\Gamma_{\rho B}^2 I_{3B} \gamma_\mu \int \frac{d^4 q}{(2\pi)^4} G_B(k+q) V_0^{\mu\nu}(q) I_{3B} \gamma_\nu. \end{aligned} \quad (4)$$

The free baryon propagator is

$$G_{B0}(k) = \frac{1}{k_\mu \gamma^\mu - m_B}, \quad (5)$$

and three free propagators of  $\sigma$ ,  $\omega$ , and  $\rho^0$  mesons, which are listed in order below:

$$D_0(q) = \frac{1}{q^2 - m_\sigma^{*2}}, \quad (6)$$

$$F_0^{\mu\nu}(q) \approx -\frac{g^{\mu\nu}}{q^2 - m_\omega^2}, \quad (7)$$

$$V_0^{\mu\nu}(q) \approx -\frac{g^{\mu\nu}}{q^2 - m_\rho^2}. \quad (8)$$

The four-momenta of neutrons and mesons are  $k \equiv (\varepsilon, \mathbf{k})$  and  $q \equiv (\omega, \mathbf{q})$ , respectively. The meson propagators are functions of both the energy and momentum, thus the DS equation (4) incorporates the dynamics of all mesons, which is neglected in mean-field theories. Moreover, we have dropped the terms  $q^\mu q^\nu / m_\omega^2$  from  $F_0^{\mu\nu}(q)$  and  $q^\mu q^\nu / m_\rho^2$  from  $V_0^{\mu\nu}(q)$  to preserve the baryon number conservation and isospin conservation, respectively. On account of the translational invariance and the rotational symmetry of infinite baryonic matter in the rest frame, we retain solely the time-component of  $\omega_\mu$  and  $\rho_\mu^3$ , which is achieved by

$$\gamma_\mu \rightarrow \gamma_0, \quad I_{3B} \gamma_\mu \rightarrow I_{3B} \gamma_0, \quad (9)$$

$$F_0^{\mu\nu}(q) \approx F_0^{00}(q), \quad V_0^{\mu\nu}(q) \approx V_0^{00}(q). \quad (10)$$

The Fermi energy  $E_{\text{FB}}$  of baryons provides a natural energy scale [64] and will be used to define the integration range of  $\omega$ . Here, we choose  $\omega \in [-\Omega_c, +\Omega_c]$ , where  $\Omega_c = 1000 \text{ MeV}$  is of the same order of  $E_{\text{FB}}$  at  $6n_{B0}$ . We have verified through numerical calculations that the EOS and NS properties are virtually insensitive to the precise value of  $\Omega_c$  for  $\Omega_c \geq 1000 \text{ MeV}$ . The absolute value of the meson momentum  $|\mathbf{q}|$  lies within the range of  $[0, \Lambda_c k_{\text{FB}}]$ , where  $k_{\text{FB}}$  is the Fermi momentum of baryon and  $\Lambda_c$  is a positive tuning parameter [64]. The parameter  $\Lambda_c$  is constrained by fitting the saturation properties of nuclear

matter. The integral measure is expressed as

$$\int \frac{d^4 q}{(2\pi)^4} \equiv \int_{-\Omega_c}^{+\Omega_c} \frac{d\omega}{2\pi} \int_0^{\Lambda_c k_{FB}} \frac{d^3 \mathbf{q}}{(2\pi)^3}. \quad (11)$$

All the results are free of divergences, thus renormalization calculations are not needed.

In infinite baryonic matter, we further assume invariance under parity and time reversal, in addition to the translational and rotational symmetries already imposed above. Under these symmetries, tensor or pseudoscalar terms are forbidden in the baryon propagator. We define three functions  $A_{0B}(k)$ ,  $A_{1B}(k)$ , and  $A_{2B}(k)$  to manifest the Landau damping, velocity renormalization, and mass renormalization, respectively. Then the baryon propaga-

tor  $G_B(k)$  can be expressed in a generic form

$$G_B(k) = \frac{1}{A_{0B}(k)\varepsilon\gamma^0 - A_{1B}(k)\mathbf{k}\cdot\boldsymbol{\gamma} - A_{2B}(k)m_B^2}. \quad (12)$$

$A_{0B}(k)$ ,  $A_{1B}(k)$ , and  $A_{2B}(k)$  are equal to unity in the non-interacting limit, but driven by baryon-meson interactions to deviate from unity. According to our numerical calculations [64],  $A_{0B}(k)$ ,  $A_{1B}(k)$ , and  $A_{2B}(k)$  exhibit a rather weak dependence on the momentum  $\mathbf{k}$  for a fixed energy. It is therefore justified [64] to fix their  $|\mathbf{k}|$  at the Fermi momentum  $k_F$ . Then,  $A_{0B}(\varepsilon)$ ,  $A_{1B}(\varepsilon)$ , and  $A_{2B}(\varepsilon)$  depend solely on the energy  $\varepsilon$ . Substituting Eq. (12) into the DS equation (4) leads to three self-consistent integral equations:

$$A_{0B}(\varepsilon) = 1 - \frac{i}{\varepsilon} \int \frac{d\omega d^3 \mathbf{q}}{(2\pi)^4} \frac{A_{0B}(\varepsilon + \omega)(\varepsilon + \omega)}{A_{0B}^2(\varepsilon + \omega)(\varepsilon + \omega)^2 - A_{1B}^2(\varepsilon + \omega)(\mathbf{k} + \mathbf{q})^2 - A_{2B}^2(\varepsilon + \omega)m_B^2} \\ \times \left( \frac{g_{\sigma B}^2}{\omega^2 - \mathbf{q}^2 - m_\sigma^{*2}} - \frac{g_{\omega B}^2}{\omega^2 - \mathbf{q}^2 - m_\omega^2} - \frac{\Gamma_{\rho B}^2 I_{3B}^2}{\omega^2 - \mathbf{q}^2 - m_\rho^2} \right), \quad (13)$$

$$A_{1B}(\varepsilon) = 1 - \frac{i}{|\mathbf{k}|} \int \frac{d\omega d^3 \mathbf{q}}{(2\pi)^4} \frac{A_{1B}(\varepsilon + \omega)|\mathbf{k} + \mathbf{q}|}{A_{0B}^2(\varepsilon + \omega)(\varepsilon + \omega)^2 - A_{1B}^2(\varepsilon + \omega)(\mathbf{k} + \mathbf{q})^2 - A_{2B}^2(\varepsilon + \omega)m_B^2} \\ \times \left( \frac{g_{\sigma B}^2}{\omega^2 - \mathbf{q}^2 - m_\sigma^{*2}} + \frac{g_{\omega B}^2}{\omega^2 - \mathbf{q}^2 - m_\omega^2} + \frac{\Gamma_{\rho B}^2 I_{3B}^2}{\omega^2 - \mathbf{q}^2 - m_\rho^2} \right), \quad (14)$$

$$A_{2B}(\varepsilon) = 1 + \frac{i}{m_B} \int \frac{d\omega d^3 \mathbf{q}}{(2\pi)^4} \frac{A_{2B}(\varepsilon + \omega)m_B}{A_{0B}^2(\varepsilon + \omega)(\varepsilon + \omega)^2 - A_{1B}^2(\varepsilon + \omega)(\mathbf{k} + \mathbf{q})^2 - A_{2B}^2(\varepsilon + \omega)m_B^2} \\ \times \left( \frac{g_{\sigma B}^2}{\omega^2 - \mathbf{q}^2 - m_\sigma^{*2}} - \frac{g_{\omega B}^2}{\omega^2 - \mathbf{q}^2 - m_\omega^2} - \frac{\Gamma_{\rho B}^2 I_{3B}^2}{\omega^2 - \mathbf{q}^2 - m_\rho^2} \right). \quad (15)$$

The three functions  $A_{0B}(\varepsilon)$ ,  $A_{1B}(\varepsilon)$ , and  $A_{2B}(\varepsilon)$  can be determined by numerical solving the above three equations using the iteration method [64]. It is challenging to compute the EOS directly from these energy-dependent functions. To simplify the calculation, we find it convenient to average over the energies of  $A_{0B}(\varepsilon)$ ,  $A_{1B}(\varepsilon)$ , and  $A_{2B}(\varepsilon)$ . The average is carried out as follows

$$\bar{A}_{0B,1B,2B} = \frac{\int A_{0B,1B,2B}(\varepsilon) d\varepsilon}{\int d\varepsilon}. \quad (16)$$

These three quantities depend on the baryon density and take into account the quantum many-body effects caused by strong baryon-meson interactions. Then the original Lagrangian density for the baryon sector, namely  $\mathcal{L}_{\text{Baryon}}$ , is renormalized to become

$$\tilde{\mathcal{L}}_{\text{Baryon}} = \sum_B \bar{\psi}_B (i\bar{A}_{0B} \partial_t \gamma^0 + i\bar{A}_{1B} \boldsymbol{\partial} \cdot \boldsymbol{\gamma} - \bar{A}_{2B} m_B \\ + g_{\sigma B} \sigma - g_{\omega B} \omega_\mu \gamma^\mu - \Gamma_{\rho B} \rho_\mu^3 I_{3B} \gamma^\mu) \psi_B. \quad (17)$$

The hyperon-meson coupling parameters are treated

following the usual approach [73]. Define several ratios:

$$x_{\sigma B} = \frac{g_{\sigma B}}{g_{\sigma N}}, \quad x_{\omega B} = \frac{g_{\omega B}}{g_{\omega N}}, \quad x_{\rho B} = \frac{g_{\rho B}}{g_{\rho N}}. \quad (18)$$

For the couplings with  $\omega$  and  $\rho^0$  mesons, we utilize the SU(6) symmetry relations [74]:

$$x_{\omega \Lambda} = x_{\omega \Sigma} = \frac{2}{3}, \quad x_{\omega \Xi} = \frac{1}{3}, \quad (19)$$

$$x_{\rho \Lambda} = x_{\rho \Sigma} = x_{\rho \Xi} = 1. \quad (20)$$

The coupling constants for hyperon- $\sigma$  meson can be obtained from hypernuclear potentials:

$$V_\Lambda = x_{\omega \Lambda} V_{\omega N} - x_{\sigma \Lambda} V_{\sigma N} = -28 \text{ MeV}, \quad (21)$$

$$V_\Sigma = x_{\omega \Sigma} V_{\omega N} - x_{\sigma \Sigma} V_{\sigma N} = +30 \text{ MeV}, \quad (22)$$

$$V_\Xi = x_{\omega \Xi} V_{\omega N} - x_{\sigma \Xi} V_{\sigma N} = -18 \text{ MeV}, \quad (23)$$

where  $V_{\omega N} = g_{\omega N} \omega_0$  and  $V_{\sigma N} = g_{\sigma N} \sigma$  are the nuclear potentials for saturated symmetric nuclear matter [75, 76]. Combining Eqs. (19-23), we can ultimately obtain

$$x_{\sigma \Lambda} = 0.5969, \quad x_{\sigma \Sigma} = 0.4223, \quad x_{\sigma \Xi} = 0.3105. \quad (24)$$

### III. EQUATION OF STATE

In this section, we calculate the EOS of the NS matter. For this purpose, we replace  $\mathcal{L}_{\text{Baryon}}$  appearing in Eq. (1) with  $\tilde{\mathcal{L}}_{\text{Baryon}}$  given by Eq. (17), and then compute the energy-density and pressure by adopting the standard procedure of RMFT [4]. The quantum many-body effects resulting from the baryon-meson interactions are already incorporated in the three averaged quantities  $\bar{A}_{0\text{B}}$ ,  $\bar{A}_{1\text{B}}$ , and  $\bar{A}_{2\text{B}}$ .

The equation of motion of the baryon field has the form

$$\begin{aligned} & [i\bar{A}_{0\text{B}}\partial_t\gamma^0 + i\bar{A}_{1\text{B}}\boldsymbol{\partial}\cdot\boldsymbol{\gamma} - \bar{A}_{2\text{B}}m_{\text{B}}] \psi_{\text{B}}(z) \\ &= -g_{\sigma\text{B}}\sigma(z)\psi_{\text{B}}(z) + g_{\omega\text{B}}\omega_{\mu}(z)\gamma^{\mu}\psi_{\text{B}}(z) \\ &\quad + \Gamma_{\rho\text{B}}\rho_{\mu}^3(z)I_{3\text{B}}\gamma^{\mu}\psi_{\text{B}}(z) + \Sigma_{\mu}^{\text{R}}\gamma^{\mu}\psi_{\text{B}}(z). \end{aligned} \quad (25)$$

where the density dependence of  $\Gamma_{\rho\text{B}}$  contributes a rearrangement term [77] for baryons:

$$\Sigma_{\mu}^{\text{R}} = \frac{J_{\mu}}{n_{\text{F}}^*} \sum_{\text{B}} \frac{\partial\Gamma_{\rho\text{B}}}{\partial n_{\text{F}}^*} \rho_{\nu}^3 \bar{\psi}_{\text{B}} I_{3\text{B}} \gamma^{\nu} \psi_{\text{B}}. \quad (26)$$

Here, the total baryon current is given by

$$J_{\mu} = \sum_{\text{B}} \bar{\psi}_{\text{B}} \gamma_{\mu} \psi_{\text{B}}, \quad (27)$$

and the total baryon density is

$$n_{\text{F}}^* = \sum_{\text{B}} n_{\text{B}}^*, \quad (28)$$

in which the renormalized baryon density of each species is

$$n_{\text{B}}^* = 2 \int_0^{k_{\text{FB}}} \frac{d^3\mathbf{k}}{(2\pi)^3} \frac{1}{\bar{A}_{0\text{B}}}. \quad (29)$$

The equations of motion of the three meson fields are of the forms:

$$(\partial_{\mu}\partial^{\mu} + m_{\sigma}^{*2})\sigma(z) = \sum_{\text{B}} g_{\sigma\text{B}}\bar{\psi}_{\text{B}}(z)\psi_{\text{B}}(z), \quad (30)$$

$$\partial_{\mu}\omega^{\mu\nu}(z) + m_{\omega}^2\omega^{\nu}(z) = \sum_{\text{B}} g_{\omega\text{B}}\bar{\psi}_{\text{B}}(z)\gamma^{\nu}\psi_{\text{B}}(z), \quad (31)$$

$$\partial_{\mu}\rho^{3\mu\nu}(z) + m_{\rho}^2\rho^{3\nu}(z) = \sum_{\text{B}} \Gamma_{\rho\text{B}}\bar{\psi}_{\text{B}}(z)I_{3\text{B}}\gamma^{\nu}\psi_{\text{B}}(z), \quad (32)$$

Then, replace the meson fields with their expectation values, namely

$$\sigma(z) \rightarrow \langle\sigma(z)\rangle = \sigma, \quad (33)$$

$$\omega_{\mu}(z) \rightarrow \langle\omega_{\mu}(z)\rangle = \omega_0, \quad (34)$$

$$\rho_{\mu}^3(z) \rightarrow \langle\rho_{\mu}^3(z)\rangle = \rho_0^3. \quad (35)$$

Then the renormalized Lagrangian density is converted to

$$\begin{aligned} \mathcal{L}^{\text{MF}} = & \sum_{\text{B}} \bar{\psi}_{\text{B}}(z) (i\bar{A}_{0\text{B}}\partial_t\gamma^0 + i\bar{A}_{1\text{B}}\boldsymbol{\partial}\cdot\boldsymbol{\gamma} - \bar{A}_{2\text{B}}m_{\text{B}} \\ & + g_{\sigma\text{B}}\sigma - g_{\omega\text{B}}\omega_0\gamma^0 - \Gamma_{\rho\text{B}}\rho_0^3 I_{3\text{B}}\gamma^0) \psi_{\text{B}}(z) \\ & - \frac{1}{2}m_{\sigma}^{*2}\sigma^2 + \frac{1}{2}m_{\omega}^2\omega_0^2 + \frac{1}{2}m_{\rho}^2(\rho_0^3)^2 \\ & + \sum_{l=e^-, \mu^-} \bar{\psi}_l (i\gamma^{\mu}\partial_{\mu} - m_l) \psi_l. \end{aligned} \quad (36)$$

The equation of motion of baryon fields, namely Eq. (25), is now simplified to

$$\begin{aligned} & [i\bar{A}_{0\text{B}}\partial_t\gamma^0 + i\bar{A}_{1\text{B}}\boldsymbol{\partial}\cdot\boldsymbol{\gamma} - g_{\omega\text{B}}\omega_0\gamma^0 - \Gamma_{\rho\text{B}}\rho_0^3 I_{3\text{B}}\gamma^0 \\ & - \Sigma_0^{\text{R}}\gamma^0 - (\bar{A}_{2\text{B}}m_{\text{B}} - g_{\sigma\text{B}}\sigma)] \psi_{\text{B}}(z) = 0, \end{aligned} \quad (37)$$

where  $\Sigma_0^{\text{R}}$  is the time component of the rearrangement term. Accordingly, Eqs. (30)-(32) are modified:

$$\sigma = \sum_{\text{B}} \frac{g_{\sigma\text{B}}}{m_{\sigma}^{*2}} \langle\bar{\psi}_{\text{B}}(z)\psi_{\text{B}}(z)\rangle = \sum_{\text{B}} \frac{g_{\sigma\text{B}}}{m_{\sigma}^{*2}} n_{\text{sB}}^*, \quad (38)$$

$$\omega_0 = \sum_{\text{B}} \frac{g_{\omega\text{B}}}{m_{\omega}^2} \langle\bar{\psi}_{\text{B}}^{\dagger}(z)\psi_{\text{B}}(z)\rangle = \sum_{\text{B}} \frac{g_{\omega\text{B}}}{m_{\omega}^2} n_{\text{B}}^*, \quad (39)$$

$$\rho_0^3 = \sum_{\text{B}} \frac{\Gamma_{\rho\text{B}}}{m_{\rho}^2} \langle\bar{\psi}_{\text{B}}^{\dagger}(z)I_{3\text{B}}\psi_{\text{B}}(z)\rangle = \sum_{\text{B}} \frac{\Gamma_{\rho\text{B}}}{m_{\rho}^2} I_{3\text{B}} n_{\text{B}}^*. \quad (40)$$

Here, a raised asterisk is used to denote the inclusion of quantum many-body effects. The renormalized scalar density is

$$n_{\text{s}}^* = \sum_{\text{B}} n_{\text{sB}}^*, \quad (41)$$

where

$$n_{\text{sB}}^* = 2 \int_0^{k_{\text{FB}}} \frac{d^3\mathbf{k}}{(2\pi)^3} \frac{m_{\text{B}}^*/\bar{A}_{0\text{B}}}{E_{\text{FB}}^*(\mathbf{k})}, \quad (42)$$

$$E_{\text{FB}}^*(\mathbf{k}) = \sqrt{\frac{\bar{A}_{1\text{B}}^2}{\bar{A}_{0\text{B}}^2}\mathbf{k}^2 + m_{\text{B}}^{*2}}, \quad (43)$$

$$m_{\text{B}}^* = \frac{\bar{A}_{2\text{B}}m_{\text{B}} - g_{\sigma\text{B}}\sigma}{\bar{A}_{0\text{B}}}. \quad (44)$$

The expectation value of the energy-momentum tensor in the rest frame of the matter is diagonal, namely

$$\langle T^{\mu\nu} \rangle = \text{diag}(\epsilon, P, P, P). \quad (45)$$

The energy density  $\epsilon = \langle T^{00} \rangle$  is

$$\begin{aligned} \epsilon = & \sum_{\text{B}} 2 \int_0^{k_{\text{FB}}} \frac{d^3\mathbf{k}}{(2\pi)^3} E_{\text{FB}}^*(\mathbf{k}) + \frac{1}{2}m_{\sigma}^{*2} \left( \sum_{\text{B}} \frac{g_{\sigma\text{B}}}{m_{\sigma}^{*2}} n_{\text{sB}}^* \right)^2 \\ & + \frac{1}{2}m_{\omega}^2 \left( \sum_{\text{B}} \frac{g_{\omega\text{B}}}{m_{\omega}^2} n_{\text{B}}^* \right)^2 + \frac{1}{2}m_{\rho}^2 \left( \sum_{\text{B}} \frac{\Gamma_{\rho\text{B}}}{m_{\rho}^2} I_{3\text{B}} n_{\text{B}}^* \right)^2 \\ & + \sum_{l=e^-, \mu^-} \frac{1}{\pi^2} \int_0^{k_l} \mathbf{k}^2 d|\mathbf{k}| \sqrt{\mathbf{k}^2 + m_l^2}, \end{aligned} \quad (46)$$

TABLE I: Simulated model parameters for the  $\sigma\omega\rho$ 2 model and the nuclear quantities computed at the saturation density within it, as developed in Ref. [64]. The experimental data for empirical nuclear quantities are:  $n_{\text{B}0} = (0.16 \pm 0.01) \text{ fm}^{-3}$ ,  $E_{\text{b}} = (-16 \pm 1) \text{ MeV}$ ,  $m_{\text{N}}^*/m_{\text{N}} = (0.56 - 0.75)$ ,  $K = (240 \pm 20) \text{ MeV}$ , and  $E_{\text{s}} = (28 - 34) \text{ MeV}$  [64]. Due to the uncertainty in the value of  $L_s$  [78], we select three values:  $L_s = 60 \text{ MeV}$ ,  $L_s = 80 \text{ MeV}$ , and  $L_s = 87.56 \text{ MeV}$  [64].

Model	$g_{\sigma\text{N}}$	$g_{\omega\text{N}}$	$g_{\rho\text{N}}$	$m_{\sigma}^*/m_{\sigma}$	$\Lambda_c$	$a_{\rho}$
$\sigma\omega\rho2L60$	17.5758	11.3153	6.5393	1.9355	1.6011	0.4097
$\sigma\omega\rho2L80$	17.5758	11.3153	6.5393	1.9355	1.6011	0.1123
$\sigma\omega\rho2L87.56$	17.5758	11.3153	6.5393	1.9355	1.6011	0.0000
	$n_{\text{B}0}(\text{fm}^{-3})$	$E_{\text{b}}(\text{MeV})$	$m_{\text{N}}^*(\text{MeV})$	$K(\text{MeV})$	$E_{\text{s}}(\text{MeV})$	$L_s(\text{MeV})$
$\sigma\omega\rho2L60$	0.1597	-16.4255	0.6462	220.5497	28.9727	60.0000
$\sigma\omega\rho2L80$	0.1597	-16.4255	0.6462	220.5497	28.9727	80.0000
$\sigma\omega\rho2L87.56$	0.1597	-16.4255	0.6462	220.5497	28.9727	87.5612

and the pressure  $P = \frac{1}{3}\langle T^{ii} \rangle$  is

$$P = \sum_B \frac{2}{3} \int_0^{k_{\text{FB}}} \frac{d^3\mathbf{k}}{(2\pi)^3} \frac{\bar{A}_{1B}^2 \mathbf{k}^2 / \bar{A}_{0B}^2}{E_{\text{FB}}^*(\mathbf{k})} - \frac{1}{2} m_{\sigma}^{*2} \left( \sum_B \frac{g_{\sigma B}}{m_{\sigma}^{*2}} n_{sB}^* \right)^2 + \frac{1}{2} m_{\omega}^2 \left( \sum_B \frac{g_{\omega B}}{m_{\omega}^2} n_B^* \right)^2 + \frac{1}{2} m_{\rho}^2 \left( \sum_B \frac{\Gamma_{\rho B}}{m_{\rho}^2} I_{3B} n_B^* \right)^2 + \sum_{l=e^-, \mu^-} \frac{1}{3\pi^2} \int_0^{k_l} d|\mathbf{k}| \frac{\mathbf{k}^4}{\sqrt{\mathbf{k}^2 + m_l^2}} + n_{\text{F}}^* \Sigma_0^{\text{R}}. \quad (47)$$

The energy density and pressure are functions of baryon density  $n_{\text{F}}^*$  through the Fermi momenta  $k_{\text{FB}}$  of each species. We have checked that the EOS satisfies the thermodynamic relationship  $P = n_{\text{F}}^{*2} \partial(\epsilon/n_{\text{F}}^*)/\partial n_{\text{F}}^*$ .

The NS cores contain, in addition to neutrons, a small fraction of protons and electrons. As the density  $n_{\text{F}}^*$  is sufficiently high, some electrons are replaced by muons when the Fermi energy of electrons surpasses the rest energy of muons. In that case, muons are energetically more favorable and the chemical potentials satisfy  $\mu_e = \mu_{\mu}$ . As the density continues to increase, hyperons could be excited in the inner core of NSs. A NS having hyperons inside is also referred to as a hyperon star (HS). The formation threshold of the baryon B can be expressed through the following relationship [4]:

$$\mu_B \geq m_B^* + g_{\omega B} \omega_0 + g_{\rho B} I_{3B} \rho_{0(3)} + \Sigma_0^{\text{R}}. \quad (48)$$

The baryon chemical potentials  $\mu_B$  are determined by the conditions of  $\beta$  equilibrium [4]

$$\mu_n = \mu_{\Lambda} = \mu_{\Xi^0} = \mu_{\Sigma^0}, \quad (49)$$

$$\mu_p = \mu_{\Sigma^+} = \mu_n - \mu_e, \quad (50)$$

$$\mu_{\Sigma^-} = \mu_{\Xi^-} = \mu_n + \mu_e, \quad (51)$$

where the chemical potentials of baryons, electrons, and

muons are given by

$$\begin{aligned} \mu_B = & \sqrt{\frac{\bar{A}_{1B}^2}{\bar{A}_{0B}^2} k_{\text{FB}}^2 + m_B^{*2}} + g_{\omega B} \left( \sum_B \frac{g_{\omega B}}{m_{\omega}^2} n_B^* \right) \\ & + g_{\rho B} I_{3B} \left( \sum_B \frac{g_{\rho B}}{m_{\rho}^2} I_{3B} n_B^* \right) + \Sigma_0^{\text{R}}, \end{aligned} \quad (52)$$

$$\mu_e = \sqrt{k_e^2 + m_e^2}, \quad (53)$$

$$\mu_{\mu} = \sqrt{k_{\mu}^2 + m_{\mu}^2}. \quad (54)$$

Here,  $k_e$  and  $k_{\mu}$  denote the Fermi momenta of electrons and muons, respectively. Notice that the many-body effects are incorporated in these chemical potentials. The lepton densities are related to the corresponding Fermi momenta via the relation  $n_{e,\mu} = k_{e,\mu}^3/(3\pi^2)$ . In addition, the NS core should obey the baryon number conservation and preserve electric charge neutrality, which are described by two identities:

$$n_{\text{F}}^* = \sum_B n_B^* = \sum_B \frac{k_{\text{FB}}^3}{3\pi^2 \bar{A}_{0B}}, \quad (55)$$

$$\sum_B Q_B + \sum_l Q_l = \sum_B \frac{q_B k_{\text{FB}}^3}{3\pi^2 \bar{A}_{0B}} - \sum_l \frac{k_l^3}{3\pi^2} = 0. \quad (56)$$

Here,  $Q_B$  and  $Q_l$  represent the electric charges carried by baryons and leptons, respectively, and  $q_B$  is the electric charge of the baryon B in units of the elementary charge. Making use of Eqs. (48-56), we determine the densities of baryons and leptons at a given total density  $n_{\text{F}}^*$ , which then generates a more realistic HS EOS that satisfies the  $\beta$  equilibrium, using Eq. (46) and Eq. (47).

#### IV. MAXIMUM MASS $M_{\text{max}}$

We adjust the six parameters  $g_{\sigma\text{N}}$ ,  $g_{\omega\text{N}}$ ,  $g_{\rho\text{N}}$ ,  $m_{\sigma}^*/m_{\sigma}$ ,  $\Lambda_c$ , and  $a_{\rho}$  to fit six typical nuclear quantities, including the nuclear saturation density  $n_{\text{B}0}$ , binding energy  $E_{\text{b}}$ , effective nucleon mass  $m_{\text{N}}^*$ , compressibility modulus  $K$ , symmetry energy  $E_{\text{s}}$ , and symmetry energy slope  $L_s$  at

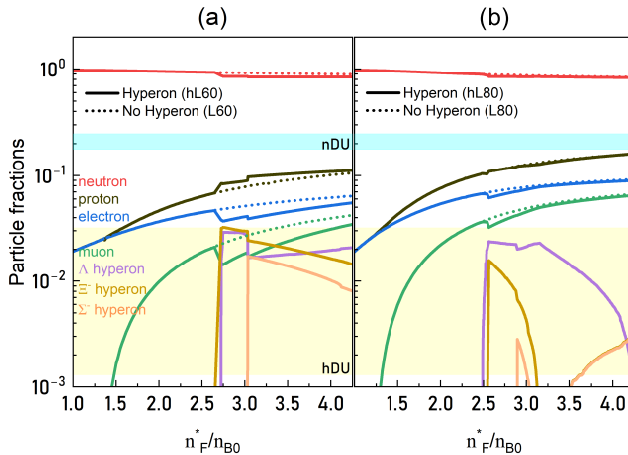


FIG. 2: Particle fractions versus baryon density  $n_F^*$  in unit of  $n_{B0}$ . The hL60 (L60) model refers to  $\sigma\omega\rho2L60$  model with (without) hyperons. The hL80 (L80) model refers to  $\sigma\omega\rho2L80$  model with (without) hyperons. Shadowed regions marked with nDU (hDU) illustrate the uncertain lower limit of the threshold fractions for nucleonic (hyperonic) DU processes.

the saturation density of symmetric nuclear matter. Table I shows that varying  $a_\rho$  does not affect the first five nuclear quantities, but has a remarkable effect on  $L_s$ . In Table I, we list three sets of adjustable parameters, referred to as  $\sigma\omega\rho2L60$  model with  $L_s = 60$  MeV,  $\sigma\omega\rho2L80$  model with  $L_s = 80$  MeV and  $\sigma\omega\rho2L87.56$  model with  $L_s = 87.56$  MeV.

We consider three hyperon species:  $\Lambda$ ,  $\Xi^-$ , and  $\Sigma^-$ . The  $\Lambda$  and  $\Xi^-$  are the first strange baryons to appear with increasing baryon density. Although  $\Sigma$  hyperons are generally disfavored by a repulsive potential [42], we include the  $\Sigma^-$  to evaluate its impact. In Fig. 2, we present the dependence of particle fractions on the normalized baryon density  $n_F^*/n_{B0}$  for four models: hL60, hL80, L60, and L80. Obviously, models with different  $L_s$ 's exhibit distinct sequences of appearance for  $\Lambda$  and  $\Xi^-$ . For hL60 model, shown in panel (a), the fractions of  $\Lambda$  and  $\Xi^-$  begin to noticeably emerge as the baryon density increases, with  $\Xi^-$  appearing at a critical density of  $2.70n_{B0}$ , followed by  $\Lambda$  at  $2.75n_{B0}$ . This sequence differs from hL80 model, shown in panel (b), in which  $\Lambda$  appears first at  $2.50n_{B0}$ , and  $\Xi^-$  emerges shortly after at  $2.55n_{B0}$ . Meanwhile, the  $\Sigma^-$  hyperon appears only at much higher densities, around  $3.00n_{B0}$ , in both hL60 and hL80 models. Hence, the value of  $L_s$  has an obvious impact on the critical density for the emergence of hyperons. Notably, even at densities above  $4n_{B0}$ , the fractions of  $\Lambda$ ,  $\Xi^-$ , and  $\Sigma^-$  all remain below 0.02, which justifies the consideration of only these three hyperons.

A comparison between the  $\epsilon$ - $P$  curves obtained for HSs (solid lines) and pure NSs (dashed lines) is depicted in Fig. 3. Clearly, the inclusion of hyperons softens the EOSs at high energy-densities. Notice that the EOSs, particularly for models with smaller values of the symmetry energy slope  $L_s$  (e.g., hL60), exhibit a dramatic abrupt softening. This behavior is caused by the sudden

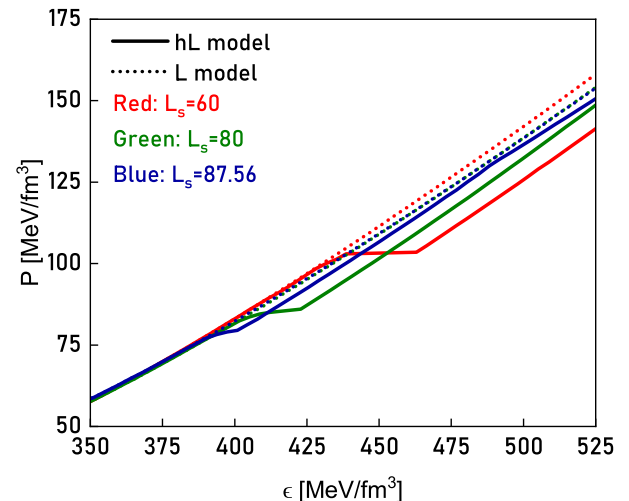


FIG. 3: Comparison between HS EOSs and NS EOSs in terms of the pressure  $P$  versus the energy-density  $\epsilon$ .

and concurrent emergence of  $\Lambda$  and  $\Xi^-$  hyperons within a narrow density interval, as illustrated by Fig. 2(a). The tuning parameter  $a_\rho$ , which governs the density dependence of isovector meson coupling parameter  $\Gamma_{\rho B}$ , plays a crucial role. As shown in Table I,  $L_s$  is reduced as  $a_\rho$  becomes larger, indicating that the symmetry energy increases more slowly with growing density. This decreases the energy cost for converting nucleons into hyperons at high densities and leads to a sudden increase in the hyperon fractions. Consequently, once the formation threshold (48) is crossed, multiple hyperon species ( $\Lambda$  and  $\Xi^-$ ) can appear almost simultaneously and their abundances rise sharply, which leads to the observed abrupt softening in the  $\epsilon$ - $P$  relation. Therefore, the parameter  $a_\rho$  regulates both the hyperon fractions and the stiffness of hyperonic matter.

The M-R relations are obtained by combining EOSs with the Tolman-Oppenheimer-Volkoff (TOV) equations [79, 80]. To construct unified EOSs, we use the CUTER v2 code [81, 82] to self-consistently reconstruct the low-density crust EOSs and match them to the high-density core EOSs, which ensures thermodynamic consistency and smoothness across the crust–core transition. In Fig. 4, we compare the M-R curves calculated based on six different models with the empirical data extracted from astrophysical observations of compact stars. Noticeably, the radii for low-mass NSs inferred from our M-R curves are in full agreement with NICER constraints on PSR J0030+0451 [83, 84]. The M-R relations predict smaller radii for low-mass NSs when  $L_s$  takes smaller values. This trend holds true irrespective of whether the hyperons are included, since the properties of low-mass NSs are nearly unaffected by hyperons that emerge at densities around  $2n_{B0}$ – $3n_{B0}$  in the NS core.

In a number of existing solutions to the hyperon puzzle based on RMFT [28, 34, 37, 51, 57, 58], the max-

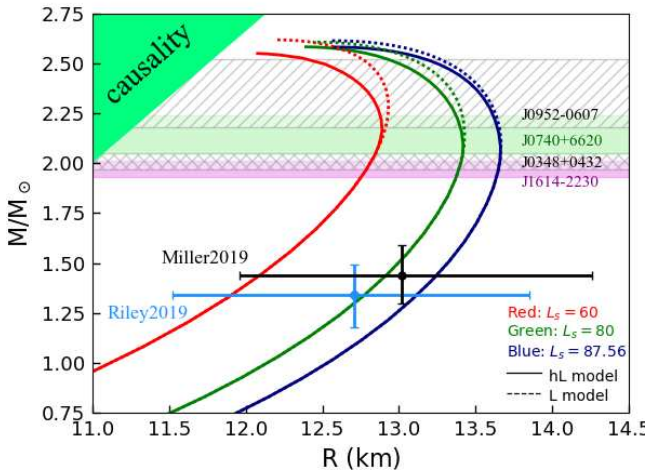


FIG. 4: Comparison between the theoretical results of M-R relations obtained from six models (hL60, hL80, hL87.56, L60, L80, and L87.56) and some recent astrophysical observations of compact stars.

imum mass  $M_{\max}$  has been elevated to the range of  $2.2M_{\odot} - 2.3M_{\odot}$  through careful selections of appropriate hyperon-meson interactions. While such a mass range suffices to explain most high-mass NSs, PSR J0952-0607 remains an exception. In a recent work [85], the high mass of PSR J0952-0607 was explained within some pure nucleonic RMFT models. These models invoke a set of extended nonlinear self- and cross-coupling terms [85] to stiffen the EOS at high densities, leading to maximum NS masses in the range  $\sim (2.34-2.50)M_{\odot}$ . As in other RMFT studies, the nonlinear terms are handled within the static Hartree approximation. These static terms furnish a classical background potential for the baryons as their quantum fluctuations are neglected. When a baryon is scattered by this potential, its energy is not changed. This implies that the baryons are nearly independent: each feels the same potential yet none affects another. The static potential shifts the baryon masses and chemical potentials, but otherwise the baryons propagate freely, forming an almost non-interacting degenerate fermion gas rather than a truly correlated quantum many-body system. After hyperons are included, the resulting EOS will be drastically softened even with the same nonlinear meson couplings [86], which decreases the maximum HS mass well below the  $\sim (2.34-2.50)M_{\odot}$  range.

Compared to those RMFT studies, our approach treats the baryon-meson interactions non-perturbatively and retain their explicit time (i.e., energy) dependence. In our scheme, all baryons are mutually correlated via the exchange of dynamical, fluctuating mesons. Quantum many-body effects enter the EOS through the averaged quantities  $\bar{A}_{0,1,2}$ , whereas the overall effect of nonlinear meson couplings is encoded in a single renormalized  $\sigma$  mass. The resulting HS EOSs are stiff enough to support a maximum mass of  $M_{\max} \approx 2.59M_{\odot}$ , even without considering stellar rotation or strong magnetic fields. This

value is more than adequate to account for the masses of several known massive NSs, including PSR J1614-2230, PSR J0348+0432, and PSR J0740+6620. Remarkably, it also supports the exceptionally high mass of PSR J0952-0607, which is challenging for other hyperonic scenarios lacking many-body effects.

Our stiff EOS still respects causality after including hyperons. Explicitly, we have verified that the sound of speed  $c_s$  is smaller than the speed of light  $c$  across all densities relevant to the stable stellar sequences in Fig. 4, irrespective of whether hyperons are present or not.

## V. FATE OF FAST COOLING

In addition to the insufficient value of  $M_{\max}$ , RMFT results face another issue about the fast cooling of HSs [30]. The proton fraction obtained from RMFT calculations typically exceeds 0.15, larger than the threshold fraction  $Y_{nDU}$  for the nucleonic DU process [56]. Meanwhile, the hyperon fractions are within the range of 0.20 – 0.60 [37, 41–44, 48–53, 58], much higher than the threshold fraction  $Y_{hDU}$  for the hyperonic DU processes [61]. A direct implication of these results is that HSs, in their early stages, would likely be significantly colder than what is inferred from astrophysical observations. This situation remains unchanged when the regulating role of baryon pairing is taken into account [62, 63]. As shown in [87], the observed age-temperature relations for dozens of NSs with low masses can be well explained by the standard cooling framework that precludes all DU processes. There are also evidences [88, 89] suggesting that the observed cooling data of many NSs can only be understood if DU processes occur in NSs with masses  $> 1.8M_{\odot}$ . In a few RMFT models, such as NL3 $\omega\rho$  [51, 59], DU processes are avoided in low-mass HSs, but they inevitably occur in HSs having high and intermediate masses. Moreover, the corresponding  $M_{\max}$  [51, 59] is not large enough to account for PSR J0952-0607.

In our scenario, the proton and hyperon fractions are substantially suppressed due to the quantum many-body effects, which is in stark contrast to RMFT results. In the absence of hyperons, a comparison between L60 and L80 models reveals that the proton fraction increases with density at a rate proportional to  $L_s$ . For  $L_s = 80$  MeV, although the proton fraction increases toward the threshold range of 0.11–0.15 [56] at higher densities, it remains below this critical interval, and is therefore insufficient to trigger the nucleonic DU process. In the case of  $L_s = 60$  MeV, however, the reduced  $L_s$  together with quantum many-body effects results in a much slower rise of the proton fraction with density. After introducing the hyperons, the proton fraction in the  $L_s = 80$  MeV model is almost unchanged, whereas in the  $L_s = 60$  MeV model it is noticeably enhanced. Nevertheless, it still remains smaller than 0.11 for all baryon densities below  $4.5n_{B0}$ , as shown in panels (a) and (b) of Fig. 2. Thus, the nucleonic DU processes are entirely inhibited. Initially,

the hyperon fractions rise after their onset and reach a maximum, but they subsequently decline with further increasing density. Eventually they stabilize below 0.02, a trend clearly shown for both values of  $L_s$ . The threshold fraction for the hyperonic DU processes is extremely low and highly uncertain, estimated to be within the range of 0.0013-0.0320 [61]. Comparing these two values reveals that the hyperonic DU processes may or may not occur in HSs. Although these processes cannot be entirely ruled out in our scenario, their likelihood of occurrence has been reduced to an unprecedentedly low level. As a result, fast cooling normally does not occur in HSs, even for those with high masses.

To understand why the neutron fraction is much higher than proton and hyperon fractions, it is useful to examine the density dependence of effective baryon masses. As shown in Fig. 5, in the absence of hyperons, the many-body effects already reduce the effective neutron mass  $m_n^*$  to small values at high densities. Once hyperons are included,  $m_n^*$  is further decreased, dropping from  $0.265m_n^*$  at  $3.00n_{B0}$  to  $0.200m_n^*$  at  $4.00n_{B0}$ . Thus, the neutrons become increasingly relativistic at higher densities. The renormalized baryon density of each species can be rephrased as

$$n_B^* = \frac{k_{FB}^3}{3\pi^2 \bar{A}_{0B}} = \frac{(\mu_B^{*2} - m_B^{*2})^{\frac{3}{2}}}{3\pi^2 \bar{A}_{1B}}. \quad (57)$$

The effective baryon chemical potential obtained from Eq. (52) is given by

$$\begin{aligned} \mu_B^* &= \mu_B - g_{\omega B} \left( \sum_B \frac{g_{\omega B}}{m_\omega^2} n_B^* \right) \\ &\quad - g_{\rho B} I_{3B} \left( \sum_B \frac{g_{\rho B}}{m_\rho^2} I_{3B} n_B^* \right) - \Sigma_0^R \\ &= \sqrt{\frac{\bar{A}_{1B}^2}{\bar{A}_{0B}^2} k_{FB}^2 + m_B^{*2}} \end{aligned} \quad (58)$$

Based on Eq. (57), one can infer that a reduction in  $m_n^*$  enhances the neutron density, which is essential to maintain a high neutron fraction. Protons display a similar trend but with a considerably higher effective mass, leading to a much lower proton fraction. The effective hyperon masses are lowered as baryon density rises, but remain above 0.65 times bare masses. Thus, hyperons are non-relativistic, which suppresses their fractions.

According to the above analysis, our current work presents a distinct prediction concerning the cooling rate of HSs, particularly those with high masses, compared to that of RMFT studies. It appears that measuring the age-temperature relations of massive HSs offers the most efficient means to verify which prediction is more reliable. The currently available observational data of such relations are rather limited and insufficient to draw a conclusive answer. It is hoped that the age-temperature relation of NSs with masses  $> 2.0M_\odot$  could be obtained with an acceptable precision in the near future. This

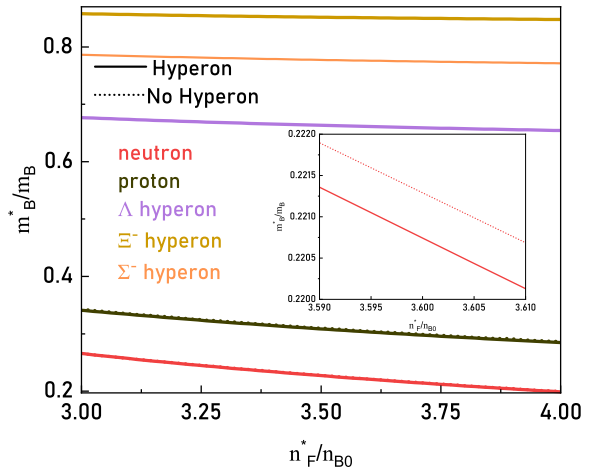


FIG. 5: Ratios of effective baryon masses to bare masses versus normalized baryon density  $n_F^*/n_{B0}$  for  $\sigma\omega\rho L80$  model.

would help determine whether the presence of hyperons in NSs necessarily leads to fast cooling.

To make the above qualitative prediction more testable, we will carry out quantitative cooling simulations in the future. These calculations would produce two sets of cooling curves for massive HSs - one without and one with quantum many-body effects. A direct comparison of the two sets of cooling curves will then allow us to quantify how many-body correlations influence the thermal evolution of HSs.

It is worth mentioning that a few exceptional NSs are observed to exhibit rapid cooling. A prominent example is the young isolated NS in the Cassiopeia A supernova remnant [90–93]. The rapid cooling of this particular NS can be attributed to the enhanced neutrino emission resulting from Cooper pairing breaking and formation [65, 66] in conjunction with the associated superfluid and superconducting quantum critical phenomena [67], without the need to invoke DU processes.

## VI. SUMMARY AND DISCUSSION

Our results demonstrate that incorporating the quantum many-body effects into the EOS of HSs not only yields a maximum mass sufficient to account for the masses of all the observed NSs, but also prevents the fast cooling induced by DU processes. Thus, our scenario provides a unified solution to the two facets of the hyperon puzzle.

While our calculated  $M_{\max} \approx 2.59M_\odot$  is already quite large, it may be further increased if the effects of NS spin [8, 94] and strong magnetic field [95] are considered. Moreover, strong magnetic field can change the particle fractions within HSs [95, 96], which would alter the conditions of DU processes. These issues will be addressed in future works. It is also interesting to apply the DS

equation framework to examine the impact of isobars on the M-R relation [41–44, 94] and other quantities.

In the present work, the DS integral equations of the renormalization functions  $A_{0,1,2}(\varepsilon)$  are solved using the bare-vertex approximation to baryon-meson couplings. With this approximation, the coupling parameters  $g_{\sigma B}$ ,  $g_{\omega B}$ , and  $g_{\rho B}$  are taken as constants. The good agreement between our results and available astrophysical observations indicates that this truncation scheme captures the essential physics of dense matter, yet upgrading to energy-momentum dependent baryon-meson vertices would yield a better description of the EOS and lead to improved results for the maximum mass and thermal evolution. Retaining the full energy-momentum dependence substantially increases the computational cost. Thus, a significantly more efficient algorithm must be developed to solve the more complicated DS equations.

## VII. ACKNOWLEDGEMENT

We thank the anonymous referees for constructive suggestions that helped improve the manuscript. H.F.Z.

thanks Wei Liu, Li Ma, Jinzhi Shen, and Zhipeng Zhang for valuable discussions on numerical calculations. G.Z.L. thanks Ang Li and Zhonghao Tu for helpful discussions. H.F.Z. and X.W. are supported by the National Natural Science Foundation of China (Grants No. 12433002 and No. 12073026). H.F.Z. is also supported by the China Postdoctoral Science Foundation (Grant No. 2025M783436). Y.F.Y. is supported by the National Natural Science Foundation of China (Grants No. 12433008, No. 12393812) and the National SKA Program of China (Grant No. 2020SKA0120300). H.F.Z., X.W., and Y.F.Y. acknowledge the support by the Cyrus Chun Ying Tang Foundations, the 111 Project for Observational and Theoretical Research on Dark Matter and Dark Energy (B23042), and Prof. Yipeng Jing's Academician Workstation. The numerical calculations in this paper have been done on the supercomputing system in the Supercomputing Center of University of Science and Technology of China.

---

[1] J. M. Lattimer and M. Prakash, The physics of neutron stars, *Science* **304**, 536 (2004).

[2] N. Yunes, M. C. Miller, and K. Yagi, Gravitational-wave and X-ray probes of the neutron star equation of state, *Nat. Rev. Phys.* **4**, 237 (2022).

[3] V. A. Ambartsumyan and G. S. Saakyan, The degenerate superdense gas of elementary particles, *Soviet Astronomy* **4**, 187 (1960).

[4] N. K. Glendenning, *Compact Stars* (Springer, Berlin, 2000).

[5] N. K. Glendenning, The hyperon composition of neutron stars, *Phys. Lett. B* **114**, 392 (1982).

[6] N.K. Glendenning, F. Weber, and S. A. Moszkowski, Neutron stars in the derivative coupling model, *Phys. Rev. C* **45**, 844 (1992).

[7] S. Balberg, I. Lichtenstadt, and G. B. Cook, Role of hyperons in neutron stars, *Astrophys. J. Suppl.* **121**, 515 (1999).

[8] Y.-F. Yuan and J. S. Heyl, Rotational evolution of protoneutron stars with hyperons: Spin up or not?, *Mon. Not. R. Astron. Soc.* **360**, 1493 (2005).

[9] J. D. Walecka, A theory of highly condensed matter, *Ann. Phys. (N.Y.)* **83**, 491 (1974).

[10] J. Boguta and A. R. Bodmer, Relativistic calculation of nuclear matter and the nuclear surface, *Nucl. Phys. A* **292**, 413 (1977).

[11] M. Dutra *et al.*, Relativistic mean-field hadronic models under nuclear matter constraints, *Phys. Rev. C* **90**, 055203 (2014).

[12] Y. Sugahara and H. Toki, Relativistic mean-field theory for unstable nuclei with non-linear  $\sigma$  and  $\omega$  terms, *Nucl. Phys. A* **579**, 557 (1994).

[13] S. Typel and H. H. Wolter, Relativistic mean field calculations with density-dependent meson-nucleon coupling, *Nucl. Phys. A* **656**, 331 (1999).

[14] C. J. Horowitz and J. Piekarewicz, Neutron star structure and the neutron radius of  $^{208}\text{Pb}$ , *Phys. Rev. Lett.* **86**, 5647 (2001).

[15] B. G. Todd-Rutel and J. Piekarewicz, Neutron-rich nuclei and neutron stars: A new accurately calibrated interaction for the study of neutron-rich matter, *Phys. Rev. Lett.* **95**, 122501 (2005).

[16] S. Typel and D. A. Terrero, Parametrisations of relativistic energy density functionals with tensor couplings, *Eur. Phys. J. A* **56**, 160 (2020).

[17] S. Typel, G. Röpke, T. Klähn, D. Blaschke, and H. H. Wolter, Composition and thermodynamics of nuclear matter with light clusters, *Phys. Rev. C* **81**, 015803 (2010).

[18] F. J. Fattoyev, C. J. Horowitz, J. Piekarewicz, and B. Reed, GW190814: Impact of a 2.6 solar mass neutron star on the nucleonic equations of state, *Phys. Rev. C* **102**, 065805 (2020).

[19] M. Dutra, O. Lourenco, and D. P. Menezes, Stellar properties and nuclear matter constraints, *Phys. Rev. C* **93**, 025806 (2016).

[20] O. Lourenço, M. Dutra, C. H. Lenzi, C. V. Flores, and D. P. Menezes, Consistent relativistic mean-field models constrained by GW170817, *Phys. Rev. C* **99**, 045202 (2019).

[21] F. Li, B.-J. Cai, Y. Zhou, W.-Z. Jiang, and L.-W. Chen, Effects of isoscalar and isovector-scalar meson mixing on neutron star structure, *Astrophys. J.* **929**, 183 (2022).

[22] K. Huang, H. Shen, J. Hu, and Y. Zhang, Hadronic equation of state of low-mass neutron stars from a relativistic mean-field model with tensor couplings, *Phys. Rev. D* **109**, 043036 (2024).

[23] S. F. Ban, J. Li, S. Q. Zhang, H. Y. Jia, J. P. Sang, and

J. Meng, Density dependencies of interaction strengths and their influences on nuclear matter and neutron stars in relativistic mean field theory, *Phys. Rev. C* **69**, 045805 (2004).

[24] P. Demorest, T. Pennucci, S. M. Ransom, M. S. E. Roberts, and J. W. T. Hessels, A two-solar-mass neutron star measured using Shapiro delay, *Nature (London)* **467**, 1081 (2010).

[25] J. Antoniadis, P. C. C. Freire, N. Wex, T. M. Tauris, R. S. Lynch, M. H. van Kerkwijk, M. Kramer, C. Bassa, V. S. Dhillon, T. Driebe, J. W. T. Hessels, V. M. Kaspi, V. I. Kondratiev, N. Langer, T. R. Marsh, M. A. McLaughlin, T. T. Pennucci, S. M. Ransom, I. H. Stairs, J. van Leeuwen *et al.*, A massive pulsar in a compact relativistic binary, *Science* **340**, 1233232 (2013).

[26] H. T. Cromartie, E. Fonseca, S. M. Ransom, P. B. Demorest, Z. Arzoumanian, H. Blumer, P. R. Brook, M. E. DeCesar, T. Dolch, J. A. Ellis, R. D. Ferdman, E. C. Ferrara, N. Garver-Daniels, P. A. Gentile, M. L. Jones, M. T. Lam, D. R. Lorimer, R. S. Lynch, M. A. McLaughlin, C. Ng *et al.*, Relativistic Shapiro delay measurements of an extremely massive millisecond pulsar, *Nat. Astron.* **4**, 72 (2019).

[27] W. H. Long, B. Y. Sun, K. Hagino, and H. Sagawa, Hyperon effects in covariant density functional theory and recent astrophysical observations, *Phys. Rev. C* **85**, 025806 (2012).

[28] G. Colucci and A. Sedrakian, Equation of state of hypernuclear matter: Impact of hyperon-scalar-meson couplings, *Phys. Rev. C* **87**, 055806 (2013).

[29] D. Lonardoni, A. Lovato, S. Gandolfi, and F. Pederiva, Hyperon puzzle: Hints from quantum Monte Carlo calculations, *Phys. Rev. Lett.* **114**, 092301 (2015).

[30] K. A. Maslov, E. E. Kolomeitsev, and D. N. Voskresensky, Solution of the hyperon puzzle within a relativistic mean-field model, *Phys. Lett. B* **748**, 369 (2015).

[31] D. Chatterjee and I. Vidaña, Do hyperons exist in the interior of neutron stars?, *Eur. Phys. J. A* **52**, 29 (2016).

[32] L. Tolos and L. Fabbietti, Strangeness in nuclei and neutron stars, *Prog. Part. Nucl. Phys.* **112**, 103770 (2020).

[33] I. Bombaci, The hyperon puzzle in neutron stars, *Nucl. Phys. News* **31**, 17 (2021).

[34] X. Sun, Z. Miao, B. Sun, and A. Li, Astrophysical implications on hyperon couplings and hyperon star properties with relativistic equations of states, *Astrophys. J.* **942**, 55 (2023).

[35] A. Chorozidou and T. Gaitanos, Momentum dependence of in-medium potentials: A solution to the hyperon puzzle in neutron stars, *Phys. Rev. C* **109**, L032801 (2024).

[36] J.-T. Ye, R. Wang, S.-P. Wang, and L.-W. Chen, High density symmetry energy: A key to the solution of the hyperon puzzle, *Astrophys. J.* **985**, 238 (2025).

[37] Z. Tu and A. Li, Delayed thermal relaxation of rapidly cooling neutron stars: Neutron superfluidity and non-nucleon particles, *Astrophys. J.* **987**, 6 (2025).

[38] J. L. Zdunik and P. Haensel, Maximum mass of neutron stars and strange neutron-star cores, *Astron. Astrophys.* **551**, A61 (2013).

[39] K. Masuda, T. Hatsuda, and T. Takatsuka, Hyperon puzzle, hadron-quark crossover and massive neutron stars, *Eur. Phys. J. A* **52**, 65 (2016).

[40] I. Bombaci, The hyperon puzzle in neutron stars, *JPS Conf. Proc.* **17**, 101002 (2017).

[41] A. Drago, A. Lavagno, and G. Pagliara, Can very compact and very massive neutron stars both exist? *Phys. Rev. D* **89**, 043014 (2014).

[42] A. Drago, A. Lavagno, G. Pagliara, and D. Pigato, Early appearance of  $\Delta$  isobars in neutron stars, *Phys. Rev. C* **90**, 065809 (2014).

[43] J. J. Li, A. Sedrakian, and F. Weber, Competition between delta isobars and hyperons and properties of compact stars, *Phys. Lett. B* **783**, 234 (2018).

[44] A. Sedrakian, J. J. Li, and F. Weber, Heavy baryons in compact stars, *Prog. Part. Nucl. Phys.* **131**, 104041 (2023).

[45] I. Vidaña, D. Logoteta, C. Providência, A. Polls, and I. Bombaci, Estimation of the effect of hyperonic three-body forces on the maximum mass of neutron stars, *Europhys. Lett.* **94**, 11002 (2011).

[46] J. Haidenbauer, U. G. Meißner, N. Kaiser, and W. Weise, Lambda-nuclear interactions and hyperon puzzle in neutron stars, *Eur. Phys. J. A* **53**, 121 (2017).

[47] D. Gerstung, N. Kaiser, and W. Weise, Hyperon-nucleon three-body forces and strangeness in neutron stars, *Eur. Phys. J. A* **56**, 175 (2020).

[48] S. Weissenborn, D. Chatterjee, and J. Schaffner-Bielich, Hyperons and massive neutron stars: Vector repulsion and SU(3) symmetry, *Phys. Rev. C* **85**, 065802 (2012).

[49] T. Miyatsu and M.-K. Cheoun, Equation of state for neutron stars in SU(3) flavor symmetry, *Phys. Rev. C* **88**, 015802 (2013).

[50] L. L. Lopes and D. P. Menezes, Hypernuclear matter in a complete SU(3) symmetry group, *Phys. Rev. C* **89**, 025805 (2014).

[51] M. Fortin, A. R. Raduta, S. Avancini, and C. Providência, Relativistic hypernuclear compact stars with calibrated equations of state, *Phys. Rev. D* **101**, 034017 (2020).

[52] S.-N. Wei, Z.-Q. Feng, and W.-Z. Jiang, Correlation of the hyperon potential stiffness with hyperon constituents in neutron stars and heavy-ion collisions, *Phys. Lett. B C* **853**, 138658 (2024).

[53] Y. Zhang, J. Hu, and P. Liu, Massive neutron star with strangeness in a relativistic mean-field model with a high-density cutoff, *Phys. Rev. C* **97**, 015805 (2018).

[54] Z. Li, Z. Ren, B. Hong, H. Lu, and D. Bai, Neutron stars within a relativistic mean field theory compatible with nucleon-nucleon short-range correlations, *Nuc. Phys.A* **990**, 118 (2019).

[55] R. W. Romani, D. Kandel, A. V. Filippenko, T. G. Brink, and W. Zheng, PSR J0952-0607: The fastest and heaviest known galactic neutron star, *Astrophys. J. Lett.* **934**, L17 (2022).

[56] J. M. Lattimer, C. J. Pethick, M. Prakash, and P. Haensel, Direct URCA process in neutron stars, *Phys. Rev. Lett.* **66**, 2701 (1991).

[57] M. Fortin, C. Providência, A. R. Raduta, F. Gulminelli, J. L. Zdunik, P. Haensel, and M. Bejger, Neutron star radii and crusts: Uncertainties and unified equations of state, *Phys. Rev. C* **94**, 035804 (2016).

[58] C. Providência, M. Fortin, H. Pais, and A. Rabhi, Hyperonic stars and the nuclear symmetry energy, *Front. Astron. Space Sci.* **6**, 13 (2019).

[59] M. Fortin, A. R. Raduta, S. Avancini, and C. Providência, Thermal evolution of relativistic hypernuclear compact stars with calibrated equations of state, *Phys. Rev. D* **103**, 083004 (2021).

[60] L. L. Lopes, Role of the symmetry energy slope in neu-

tron stars: Exploring the model dependency, *Phys. Rev. C* **110**, 015805 (2024).

[61] M. Prakash, M. Prakash, J. M. Lattimer, and C. J. Pethick, Rapid cooling of neutron stars by hyperons and  $\Delta$  isobars, *Astrophys. J.* **390**, L77 (1992).

[62] D. G. Yakovlev, A. D. Kaminker, O. Y. Gnedin, and P. Haensel, Neutrino emission from neutron stars. *Phys. Rep.* **354**, 1 (2001).

[63] D. Page, J. M. Lattimer, M. Prakash, and A. W. Steiner, Minimal cooling of neutron stars: A new paradigm. *Astrophys. J. Suppl. Ser.* **155**, 623 (2004).

[64] H.-F. Zhu, X. Wu, and G.-Z. Liu, Nonperturbative study of quantum many-body correlation effects in neutron stars: Equation of state, *Phys. Rev. C* **110**, 035810 (2024).

[65] D. Page, M. Prakash, J. M. Lattimer, and A. W. Steiner, Rapid cooling of the neutron star in Cassiopeia A triggered by neutron superfluidity in dense matter, *Phys. Rev. Lett.* **106**, 081101 (2011).

[66] P. S. Shternin, D. G. Yakovlev, C. O. Heinke, W. C. G. Ho, and D. J. Patnaude, Cooling neutron star in the Cassiopeia A supernova remnant: Evidence for superfluidity in the core, *Mon. Not. R. Astron. Soc.* **412**, L108 (2011).

[67] H.-F. Zhu, G.-Z. Liu, and X. Wu, Rapid cooling of the Cassiopeia A neutron star due to superfluid quantum criticality, *arXiv:2410.21945* (2024).

[68] K. Oyamatsu and K. Iida, Symmetry energy at subnuclear densities and nuclei in neutron star crusts, *Phys. Rev. C* **75**, 015801 (2007).

[69] R. Cavagnoli, D. P. Menezes, and C. Providênciâ, Neutron star properties and the symmetry energy, *Phys. Rev. C* **84**, 065810 (2011).

[70] F. Grill, C. Providênciâ, and S. S. Avancini, Neutron star inner crust and symmetry energy, *Phys. Rev. C* **85**, 055808 (2012).

[71] F. Ji, J. Hu, S. Bao, and H. Shen, Effects of nuclear symmetry energy and equation of state on neutron star properties, *Phys. Rev. C* **100**, 045801 (2019).

[72] X. Wu, S. Bao, H. Shen, and R. Xu, Effect of the symmetry energy on the secondary component of GW190814 as a neutron star, *Phys. Rev. C* **104**, 015802 (2021).

[73] M. Chiapparini, M. E. Bracco, A. Delfino, M. Malheiro, D. P. Menezes, and C. Providênciâ, Hadron production in non-linear relativistic mean field models, *Nuc. Phys. A* **826**, 178 (2009).

[74] C. B. Dover and A. Gal, Hyperon-nucleus potentials, *Prog. Part. Nucl. Phys.* **12**, 171 (1984).

[75] J. Schaffner-Bielich, M. Hanauske, H. Stöcker, and W. Greiner, Phase transition to hyperon matter in neutron stars, *Phys. Rev. Lett.* **89**, 171101 (2002).

[76] E. Friedman and A. Gal, In-medium nuclear interactions of low-energy hadrons, *Phys. Rep.* **452**, 89 (2007).

[77] H. Lenske and C. Fuchs, Rearrangement in the density dependent relativistic nuclei, *Phys. Lett. B* **345**, 355 (1995).

[78] S. Tagami, T. Wakasa, and M. Yahiro, Slope parameters determined from CREX and PREX2, *Results in Physics* **43**, 106037 (2022).

[79] R. C. Tolman, Static solutions of Einstein's field equations for spheres of fluid, *Phys. Rev.* **55**, 364 (1939).

[80] J. R. Oppenheimer and G. M. Volkoff, On massive neutron cores, *Phys. Rev.* **55**, 374 (1939).

[81] P. J. Davis, H. D. Thi, A. F. Fantina, F. Gulminelli, M. Oertel, and L. Suleiman, Inference of neutron-star properties with unified crust-core equations of state for parameter estimation, *Astron. Astrophys.* **687**, A44 (2024).

[82] P. J. Davis, H. D. Thi, A. F. Fantina, F. Gulminelli, M. Oertel, and L. Suleiman, Crust (unified) tool for equation-of-state reconstruction (CUTER) v2, *Eur. Phys. J. A* **61**, 120 (2025).

[83] M. C. Miller, F. K. Lamb, A. J. Dittmann, S. Bogdanov, Z. Arzoumanian, K. C. Gendreau, S. Guillot, A. K. Harding, W. C. G. Ho, J. M. Lattimer, R. M. Ludlam, S. Mahmoodifar, S. M. Morsink, P. S. Ray, T. E. Strohmayer, K. S. Wood, T. Enoto, R. Foster, T. Okajima, G. Prigozhin, and Y. Soong, PSR J0030+0451 mass and radius from NICER data and implications for the properties of neutron star matter, *Astrophys. J. Lett.* **887**, L24 (2019).

[84] T. E. Riley, A. L. Watts, S. Bogdanov, P. S. Ray, R. M. Ludlam, S. Guillot, Z. Arzoumanian, C. L. Baker, A. V. Bilous, D. Chakrabarty, K. C. Gendreau, A. K. Harding, W. C. G. Ho, J. M. Lattimer, S. M. Morsink, and T. E. Strohmayer, A NICER view of PSR J0030+0451: Millisecond pulsar parameter estimation, *Astrophys. J. Lett.* **887**, L21 (2019).

[85] R. Kumar, M. Kumar, V. Thakur, S. Kumar, P. Kumar, A. Sharma, B. K. Agrawal, and S. K. Dhiman, Observational constraint from the heaviest pulsar PSR J0952-0607 on the equation of state of dense matter in relativistic mean field model, *Phys. Rev. C* **107**, 055805 (2023).

[86] S. K. Dhiman, R. Kumar, and B. K. Agrawal, Nonrotating and rotating neutron stars in the extended field theoretical model, *Phys. Rev. C* **76**, 045801 (2007).

[87] A. Y. Potekhin, D. A. Zyuzin, D. G. Yakovlev, M. V. Beznogov, and Yu. A. Shibanov, Thermal luminosities of cooling neutron stars, *Mon. Not. R. Astron. Soc.* **496**, 5052 (2020).

[88] R. Negreiros, L. Tolos, M. Centelles, A. Ramos, and V. Dexheimer, Cooling of small and massive hyperonic stars, *Astrophys. J.* **863**, 104 (2018).

[89] A. R. Raduta, A. Sedrakian, and F. Weber, Cooling of hypernuclear compact stars, *Mon. Not. R. Astron. Soc.* **475**, 4347 (2018).

[90] W. C. G. Ho and C. O. Heinke, A neutron star with a carbon atmosphere in the Cassiopeia A supernova remnant, *Nature (London)* **462**, 71 (2009).

[91] C. O. Heinke and W. C. G. Ho, Direct observation of the cooling of the Cassiopeia a neutron star, *Astrophys. J. Lett.* **719**, L167 (2010).

[92] B. Posselt and G. G. Pavlov, Upper limits on the rapid cooling of the central compact object in Cas A, *Astrophys. J.* **864**, 135 (2018).

[93] B. Posselt and G. G. Pavlov, The cooling of the central compact object in Cas A from 2006 to 2020, *Astrophys. J.* **932**, 83 (2022).

[94] F. M. da Silva, A. Issifu, L. C. N. Santos, T. Frederico, and D. P. Menezes, Hyperons and  $\Delta$ 's in rotating protoneutron stars I: global properties, *Phys. Rev. D* **112**, 023007 (2025).

[95] A. E. Broderick, M. Prakash, and J. M. Lattimer, Effects of strong magnetic fields in strange baryonic matter, *Phys. Lett. B* **531**, 167 (2002).

[96] P. Yue, F. Yang, and H. Shen, Properties of hyperonic matter in strong magnetic fields, *Phys. Rev. C* **79**, 025803 (2009).